Spectral Analysis of Cardiogenic Vibrations to Distinguish Between Valvular Heart Diseases

Ecem Erin[1] and Beren Semiz[2] [a]

[1]*Department of Physics, Bogazici University, Istanbul, Turkey*
[2]*Department of Electrical and Electronics Engineering, Koc University, Istanbul, Turkey*

Keywords: Seismocardiogram, Cardiovascular Health Monitoring, Valvular Heart Disease, Biomedical Signal Processing.

Abstract: Cardiovascular diseases are one of the top causes of mortality, accounting for a sizeable portion of all fatalities globally. Among cardiovascular diseases, valvular heart diseases (VHDs) affect greater number of people and have higher mortality rates. Current VHD assessment methods are cost-inefficient and limited to clinical settings, therefore there is a compelling need for non-invasive and continuous VHD monitoring systems. In this work, a novel framework was proposed to distinguish between aortic stenosis (AS), aortic valve regurgitation (AR), mitral valve stenosis (MS), and mitral valve regurgitation (MR) using tri-axial seismocardiogram (SCG) signals acquired from the mid-sternum. First, seismology domain knowledge was leveraged and applied to SCG signals through ObsPy toolbox for pre-processing. From pre-processed signal segments, spectrogram, wavelet, chromagram, tempogram and zero-crossing-rate features were extracted. Following p-value analysis and variance thresholding, a multi-label/multi-class classification framework based on gradient boosting trees was developed to distinguish between AS, AR, MS and MR cases. For all four VHDs, the accuracy, precision, recall and f1-score values were above 95%, best performing axis being the dorso-ventral direction. Overall, the results showed that spectral analysis of SCG signals can provide valuable information regarding VHDs and potentially be used in the design of continuous monitoring systems.

1 INTRODUCTION

Today, diagnosis and treatment titration for any disease or injury are generally achieved with conventional biomarkers, of which derivation requires frequent hospital visits and expensive laboratory tests (Meister et al., 2016). This causes an information gap regarding the physiological changes occurring between subsequent hospital visits, and it becomes mandatory to resort to reactive treatment policies as early diagnosis and intervention are often not possible (Golubnitschaja et al., 2014). Thus, there is a compelling need for wearable sensor systems and analysis frameworks to digitize these indicators and to achieve continuous health monitoring.

The World Health Organization's 2020 report lists cardiovascular diseases as one of the top causes of mortality, accounting for a sizeable portion of all fatalities globally (WHO, 2020). Among cardiovascular diseases, valvular heart diseases (VHDs) affect greater number of people and have higher mortal-

ity rates (Go et al., 2013). VHDs emerge from the impairments of the heart valves, i.e. the pulmonary valve, the tricuspid valve, the aortic valve, and the mitral valve (Klabunde, 2011; Svensson, 2008). These impairments can be listed under two main groups: stenosis and regurgitation, which can be observed in any of these four valves. In stenosis case, the valvular orifice narrows down, resulting in insufficient outflow of blood; whereas regurgitation corresponds to the incompetence of the valve in preventing backflow of blood (Svensson, 2008). Although the VHDs can be monitored through magnetic resonance imaging, echocardiography, computed tomography and cardiac catheterization, these methods are cost inefficient and limited to clinical settings (Svensson, 2008).

As physiological signals recorded from the human body directly emerge from the biological mechanisms, they can provide clinically useful information about the underlying processes and pathological conditions. Among these signals, seismocardiogram (SCG) signal is one of the most popular ones leveraged in wearable system design. SCG represents the mechanical activity of the heart and reflects the lo-
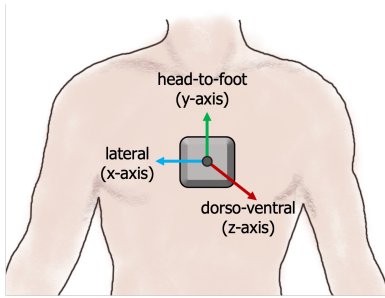
[a] https://orcid.org/0000-0002-7544-5974

Figure 1: The X, Y, and Z axes were corresponding to lateral, head-to-foot, and dorso-ventral axes, respectively.

Table 1: Dataset Description.

	Number of Subjects
Only MS	3
Only MR	13
Only AR	5
Only AS	16
MS and AS	3
AR and AS	1
MR and AR	6
MR and AS	3
MS and MR	1
MS, MR and AS	1
MS, MR and AR	1
MR, AR and AS	1
MS, MR, AR, and AS	2

cal chest vibrations originating from the contraction of the heart (Inan et al., 2014). Previous studies have shown that the SCG signal can be leveraged in the detection of aortic stenosis (Yang et al., 2019), heart failure (Inan et al., 2018), and atrial fibrillation (Hurnanen et al., 2016), as well as estimating systolic time intervals (Shandhi et al., 2019), predicting stroke volume values (Semiz et al., 2020) and assessing respiration phases (Imirzalioglu and Semiz, 2022; Pandia et al., 2012). To the best of our knowledge, there is no study in the literature which focuses on distinguishing between different VHDs using SCG signals.

The SCG signal has indeed have close similarities with the seismograph signal, which represents the recording of vibrations in the Earth to assess earthquake incidences (Lay and Wallace, 1995). As they both measure *vibrations*, it can be proposed that the pre-processing methods used in the analysis of seismograph signal can facilitate the analysis of SCG signals. Accordingly, first the seismology domain analysis has been inherited through the *ObsPy* framework for pre-processing (Beyreuther et al., 2010). In addition, recent studies have primarily focused on analyzing the SCG signals in time domain, i.e. analysis of the peak- and valley-related features. However, the frequency domain analysis of SCG signals has been less studied. Thus, in the presented work, following ObsPy analysis, the signals were additionally investigated in frequency domain through spectrogram, wavelet, chromagram and tempogram analysis.

The contributions of this study can be listed as follows: (i) For the first time to the best of our knowledge, a pipeline was presented to distinguish between aortic stenosis (AS), aortic valve regurgitation (AR), mitral valve stenosis (MS), and mitral valve regurgitation (MR) using the tri-axial SCG signals collected from the mid-sternum. In this novel analysis pipeline, (ii) seismology domain knowledge was inherited and applied to the SCG signals for pre-processing, and (iii) spectral-domain analysis was leveraged to investigate the relationship between frequency domain characteristics of the SCG signals and VHDs.

2 METHODS

2.1 Dataset Description

In this paper, *An Open-Access Database for the Evaluation of Cardio-Mechanical Signals From Patients With Valvular Heart Disease* was used (Yang et al., 2021). Dataset includes SCG, gyrocardiogram (GCG) and electrocardiogram (ECG) signals from 100 patients collected at Columbia University Medical Center (USA), Stevens Institute of Technology (USA), Southeast University (China), Nanjing Medical University (China) and Nanjing Medical University (China). Subjects were diagnosed with various conditions of valvular heart diseases (VHD), such as aortic stenosis (AS), aortic valve regurgitation (AR), mitral valve stenosis (MS), mitral valve regurgitation (MR), and tricuspid valve regurgitation (TR). The presence and non-presence of each VHD was labeled with 1 and 0, respectively. It should be noted that most of the subjects were labeled with more than 1 VHD. Subject demographics were as follows: age = 68 ± 14 years, height = 165 ± 9 cm, weight = 69 ± 13 kg.

To collect ECG, SCG and GCG signals, an off-the-shelf sensor (Shimmer 3 ECG module, Shimmer Sensing, United Kingdom) was used. Subjects were asked to stay motionless in supine position while the data was being recorded. For the analysis, only the tri-axial SCG signal was used. As shown in Fig. 1, the X, Y, and Z directions of the SCG signal were corresponding to the lateral, head-to-foot, and dorso-ventral directions, respectively. As there was no subject having only TR, subjects having TR in addition to other VHD were excluded. Number of VHD cases included in the analysis is summarized in Table 1.
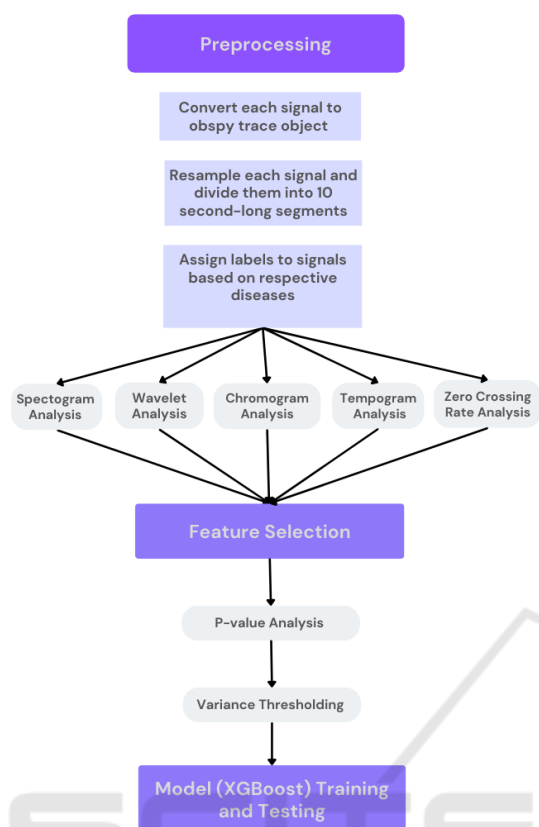
Figure 2: Block diagram for the proposed framework. First, detrending, tapering, resampling and segmentation were applied on the signals. Spectrogram, wavelet, chromagram, tempogram and zero crossing rate features were then extracted from each segment. Following p-value and variance thresholding, a multi-label/multi-output classification model was trained and tested using the remaining features.

2.2 Pre-processing of the SCG Signals

As the seismological data and vibrations on the chest wall have a similar mechanism, SCG signals show close resemblance to the seismograph signal. Hence, biomedical signal processing knowledge was combined with the tools available for seismograph analysis. To that end, the use of ObsPy toolbox, which allows manipulation and processing of seismograph signals (Beyreuther et al., 2010), was leveraged. Indeed, using ObsPy let the SCG signal characteristics (such as sampling rate, number of points and durations) be more easily accessible. More importantly, employment of manual and heuristic pre-processing and feature extraction methods could be avoided.

Previous studies have shown that SCG analysis highly benefits from the features extracted from all three axes (dorso-ventral, lateral and head-to-foot); hence, in this study, all three axes were included in the analysis (Semiz et al., 2020). While transform-

ing these signals into traces, each signal was first detrended linearly to remove unwanted baseline oscillations. Detrended waveforms were then tapered with "Hann" window having a decimal percentage of 0.05 to prepare them for frequency analysis. In the dataset, some signals had a sampling rate of 512 Hz while the sampling rate for others were 256 Hz. As a solution, all sampling rates were set to 256 Hz using Obspy's resampling method. As the final step, each signal was divided into 10-second long segments to increase the number of instances. This resulted in a total of 2393 segments (instances).

2.3 Feature Extraction

Following aforementioned pre-processing steps, feature extraction was performed on the SCG signals. To that aim, spectrogram, wavelet, chromagram and tempogram features were extracted from each 10-second-long X, Y, Z segment. Additionally, zero crossing rate analysis was leveraged as zero crossings were found correlated with the spectral centroid and dominant frequencies (Koutroumbas and Theodoridis, 2008).

2.3.1 Spectrogram Analysis

A spectrogram is a two-dimensional function of frequency and time that depicts how a non-stationary signal's frequency content changes over time (McClellan et al., 2003). Hence, spectrogram analysis can provide useful information regarding the time-dependent variances observed in the spectrum.

In this work, spectrogram analysis was employed using ObsPy's spectrogram function, with a slight modification in the output. The original function was outputting the spectrogram images, i.e., the combination of coefficients, frequency values and time instances. However, for this study, only the spectrogram coefficients were required to be used as features. That is why, time average of the coefficients for each frequency band was calculated and stored as a vector. This was repeated for each of the 10-second-long segment, i. In the end, a matrix $\mathbf{S}_i = (\mathbf{S}_{x,i}, \mathbf{S}_{y,i}, \mathbf{S}_{z,i})$ was generated, which includes time-averaged spectrogram coefficients for each of the lateral, head-to-foot and dorso-ventral axes of segment i.

2.3.2 Wavelet Analysis

Physiological signals show time-varying statistics due to their dynamic nature. As wavelet transform allows for the analysis of non-stationary signals (e.g. biomedical signals) at multiple scales, it was also found to be an effective approach for this study. In

wavelet analysis, the signal is decomposed into a collection of basis functions using a finite-length function called *mother wavelet*. Indeed, there are many different mother wavelets available depending on the application. The width and central frequency of the mother wavelet can be adjusted by moving it through the signal-of-interest. These shifted and scaled versions of the mother wavelet are also known as *daughter wavelets* (Polikar, 1996).

In this work, 1D multilevel discrete wavelet transformation with a level-6 *sym5* wavelet was employed. Having 6 levels ensured that the signal was decomposed up until the respiration band (Pandia et al., 2012). On the other hand, *sym5* was chosen as it shows morphological similarities with the SCG signals and has been one of the most popular mother wavelets used in biomedical signal analysis (Jahromi et al., 2017).

The output was including the approximation coefficients (a_6) and 6-levels of detail coefficients (d_1, d_2, d_3, d_4, d_5 and d_6). Considering that the sampling rate was set to 256 Hz, the maximum frequency available in the signals was 128 Hz. Thus, the frequency ranges of the detail coefficients were 64-128 Hz, 32-64 Hz, 16-32 Hz, 8-16 Hz, 4-8 Hz, and 2-4 Hz, which correspond to d_1, d_2, d_3, d_4, d_5 and d_6 coefficients, respectively (Fig. 3). On the other hand, a_6 was representing the 0-2 Hz frequency band. The detail and approximation coefficients were extracted for all three axes and concatenated together. In the end, a matrix $\mathbf{W}_i = (\mathbf{W}_{x,i}, \mathbf{W}_{y,i}, \mathbf{W}_{z,i})$, was generated, which includes concatenated approximation and detail coefficients for each of the lateral, head-to-foot and dorso-ventral axes of segment i.

2.3.3 Chromagram Analysis

In recent years, there have been great advancements in audio analysis thanks to the semantic analysis (Shah et al., 2019). Chroma features have found to be powerful representations of any audio as they can be used to generate audio fingerprints. Chroma features measure the dominance of the characteristics of a certain pitch (*C*, *C#*, *D*, *D#*, *E*, *F*, *F#*, *G*, *G#*, *A*, *A#* or *B*) in signal-of-interest. To compute chroma features, instantaneous frequency estimates from the spectrogram were taken to obtain high-resolution chroma profiles (Giannakopoulos and Pikrakis, 2014).

Recently, it has been shown that biomedical signal processing can highly benefit from audio analysis methods, more specifically from chroma features (Hersek et al., 2017). Similarly, in this work, chroma features corresponding to aforementioned 12 pitch values were extracted from each signal segment. After extracting pitch values, their time-average was
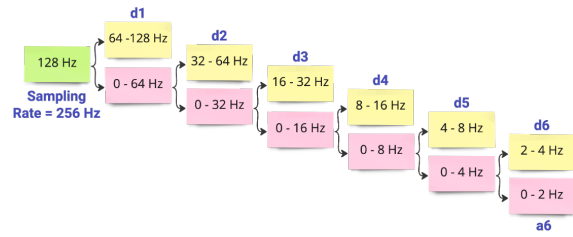

Figure 3: 6-Level wavelet decomposition. 6-Levels of detail coefficients: d_1, d_2, d_3, d_4, d_5 and d_6. 6th Level approximation coefficient: a_6.

computed to have one single value for each pitch. These steps were repeated for all three axes. In the end, a matrix $\mathbf{C}_i = (\mathbf{C}_{x,i}, \mathbf{C}_{y,i}, \mathbf{C}_{z,i})$, was generated which includes time-averaged pitch values for each of the lateral, head-to-foot and dorso-ventral axes of segment i.

2.3.4 Tempogram Analysis

As mentioned in Section 2.3.3, it has been shown that biomedical signal processing can highly benefit from audio analysis methods (Hersek et al., 2017). That is why in addition to chromagram features, tempogram analysis was also leveraged in the analysis. Tempo and beat, which are components of rhythm, can be used to distinguish audio from each other. Unlike beat, tempo can vary locally within an audio. Hence using tempogram, information regarding tempo at each time instance can be obtained.

From each signal segment, tempogram features were computed using a hop length and sampling rate of 256 Hz each. Tempogram coefficients were then averaged within each window. These steps were again repeated for all three axes. In the end, a matrix $\mathbf{T}_i = (\mathbf{T}_{x,i}, \mathbf{T}_{y,i}, \mathbf{T}_{z,i})$, was generated which includes averaged tempogram values for each of the lateral, head-to-foot and dorso-ventral axes of segment i.

2.3.5 Zero-Crossing Rate Analysis

Zero crossing rate (ZCR) represents the rate of sign-changes of the signal-of-interest (Giannakopoulos and Pikrakis, 2014). It is generally used to evaluate the signal's noise level, i.e., ZCR values tend to increase as noise levels increases. On the other hand, ZCR was found to be correlated with the spectral centroid and dominant frequencies (Koutroumbas and Theodoridis, 2008). Hence, ZCR value for each segment was included as a feature in the analysis. For the 10-second-long segments, ZCR was calculated for each of the X, Y, Z axes. In the end, a matrix $\mathbf{Z}_i = (z_{x,i}, z_{y,i}, z_{z,i})$ was generated where each row refers to one 10-second-long segment, i, and ($z_{x,i}$, $z_{y,i}$, $z_{z,i}$) repre-

sent the ZCR values of X, Y, Z axes for segment i.

2.3.6 Data Frame Generation

After the aforementioned features were extracted from each segment, one single data frame was formed for ease of feature selection and model training. First, the VHD labels were organized to make the data ready for multi-label classification. To that aim, corresponding VHD label vectors in the form [AR, AS, MR, MS] were generated and assigned to each 10-second long segment. The presence of each VHD was labeled with 1 and non-presence was indicated with 0. For example, let us assume that the subject had AR and MR, however did not have AS or MS. Then the corresponding label vector was formed as [1,0,1,0]. Similarly if a subject had MS, bu no other VHDs, the vector was formed as [0,0,0,1]. These label vectors were generated for each of the 10-second-long segments, eventually leading to a matrix $\mathbf{L}$, where each row represents the label vector for one segment.

Following label generation, previously generated feature matrices and the label matrix were concatenated altogether to have one single frame where each row corresponds to one 10-second long segment. In the end, the dataframe had the following structure: $[\mathbf{S}_i, \mathbf{W}_i, \mathbf{C}_i, \mathbf{T}_i, \mathbf{Z}_i, \mathbf{L}_i]$, where $\mathbf{S}_i, \mathbf{W}_i, \mathbf{C}_i, \mathbf{T}_i, \mathbf{Z}_i$, are the spectrogram, wavelet, chromagram, tempogram and zero crossing rate features, respectively; and $\mathbf{L}_i$ is the corresponding VHD vector for segment i.

2.4 Feature Selection

Following feature extraction, the data frame was including 7497 features in total. However this would cause curse of dimensionality, i.e., the vector space would be sparser due to an increase in dimensionality (Chen, 2009). This would potentially hurt the training/learning phase and lead to overfitting; hence, multi-step feature selection was employed. First, Mann-Whitney U test with an alpha level of 0.05 was applied to the generated dataframe. In other words, any feature having a p-value smaller than 0.05 was accepted statistically significant. After removing the features having p > 0.05, variance thresholding was employed with a threshold of 0.0001. Both methods are detailed in the following subsections.

2.4.1 p-value Analysis

For p-value-based feature selection, Mann-Whitney U test with an alpha value of 0.05 was implemented. Mann-Whitney U test falls under non-parametric hypothesis tests, i.e., it does not make any assumption

regarding the distribution of the data unlike parametric tests, which assume normal distribution in the data. Hence, Mann-Whitney U test was determined as the feature selection method (Sedgwick, 2015).

While performing the test, instead of comparing the feature variances of the diseases altogether, features corresponding to different diseases were compared pair-wise. For example, the spectrogram coefficients of AR were compared with the spectrogram coefficients of AS, MR and MS one by one (e.g. ($[\mathbf{S}_{AR_i}]$ vs. $[\mathbf{S}_{AS_i}]$), ($[\mathbf{S}_{AR_i}]$ vs. $[\mathbf{S}_{MR_i}]$), ($[\mathbf{S}_{AR_i}]$ vs. $[\mathbf{S}_{MS_i}]$), etc.). This comparison was repeated for all combinations. During each comparison, any feature column with p value > 0.05 was eliminated and the remaining columns were used in the analysis. As a result, total number of columns decreased from 7497 to 763.

2.4.2 Variance Thresholding

Following p-value analysis, variance thresholding was applied on the remaining 763 columns to eliminate the redundant features further. Variance thresholding is one of the filter-based methods and aims to drop the features having variance values below a predetermined threshold (Bommert et al., 2020). Features with lower variance indeed carry less information, since their variance is proportional to the level of predictive power they have. Accordingly, the variance of each feature was calculated and a threshold of 0.0001 was applied. As a result, the total number of features was decreased from 763 to 308.

2.5 Model Training and Validation

2.5.1 Classification Framework and Performance Metrics

To establish a multi-label/multi-output classification framework, label vectors were generated as previously explained in Section 2.3.6. The framework was built using *One vs. Rest* approach. As the classification model, Extreme Gradient Boosting Trees (XGBoost) was leveraged. XGBoost falls under ensemble methods, i.e., instead of a single estimator, multiple estimators are simultaneously used to predict a variable. During training, multiple decision trees are iteratively trained, so that residual errors from the previous iteration can be predicted and improved over time (Dieterich et al., 2002).

In this work, 80% of the data was used for training process and 20% was used for testing. During training, the objective function was determined to be *binary:logistic*, whereas other parameters were kept in their default values. The performance of the model was assessed using accuracy, precision, recall, and

Table 2: Classification Results.

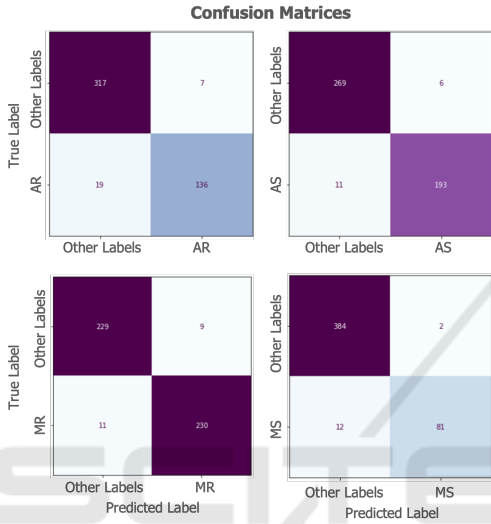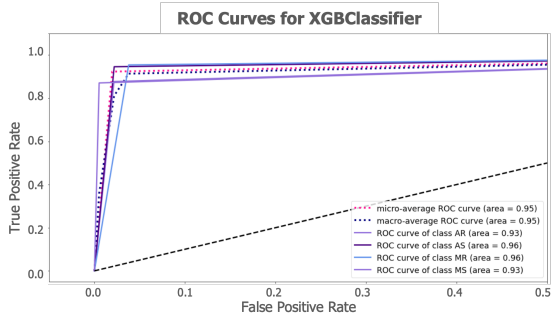|	AR	AS	MR	MS
Accuracy	0.95	0.96	0.96	0.97
Precision (macro)	0.95	0.97	0.96	0.97
Precision (weighted)	0.95	0.96	0.96	0.97
Recall (macro)	0.93	0.96	0.96	0.93
Recall (weighted)	0.95	0.96	0.96	0.97
f1-score (macro)	0.94	0.96	0.96	0.95
f1-score (weighted)	0.95	0.96	0.96	0.97
ROC AUC	0.93	0.96	0.96	0.93

Figure 4: ROC curves and confusion matrices.

f1-score metrics for each of the AR, AS, MR, and MS classes. The corresponding equations were listed in Equations 1, 2, 3, 4, respectively (*TP: true positives, FP: false positives, TN: true negatives and FN: false negatives*). In addition, the areas under the receiver operating characteristics curve (ROC AUC) were computed for each disease.

$$Accuracy = \frac{TP + TN}{TP + TN + FP + FN} \quad (1)$$

$$Precision = \frac{TP}{TP + FP} \quad (2)$$

$$Recall = \frac{TP}{TP + FN} \quad (3)$$

$$f_1 score = 2 * \frac{precision * recall}{precision + recall} \quad (4)$$

2.5.2 Axis Interpretation

As an additional analysis, the X, Y and Z axes features were investigated individually to assess the contribution of each axis. To that aim, similar feature extraction, feature selection and model training steps

were leveraged, i.e., (i) The spectrogram, wavelet, tempogram, chromagram and zero crossing rate features were first assessed using p-value analysis and variance thresholding. (ii) A multi-label/multi-output model was then trained and tested using the remaining features. These steps were employed on each of the X, Y and Z axes. The performance of the models were again assessed using accuracy, precision, recall, f1-score and ROC AUC metrics.

3 RESULTS AND DISCUSSION

3.1 Feature Selection

In the first part of the analysis, the combination of the features extracted from all three SCG axes was used. First, the number of features was decreased from 7497 to 308 using a cascaded feature selection pipeline including p-value analysis and variance thresholding. One important observation was that out of the wavelet features, only the approximation coefficients, which correspond to the 0 - 2 Hz, could reject the null hypothesis and be included in the final feature set. This band primarily represents the respiration information as the frequencies below 1 Hz are associated with the chest movements originating from exhalation and inhalation phases (Pandia et al., 2012). In the literature, it has been shown that respiration has an indisputable effect on cardiac murmurs as the change in murmur intensity during breathing can provide valuable information regarding the origin and pathological significance of the murmur (Levin et al., 1962). Hence, these findings were indeed consistent with the underlying physiological processes. Another important observation was that all zero-crossing-rate features from all three axes could reject the null hypothesis, thus it can be deduced that different VHDs induce different amounts of sign change on the SCG signals. This difference can be attributed to either the differences in induced noise or effects on spectral components as previously discussed (Giannakopoulos and Pikrakis, 2014; Koutroumbas and Theodoridis, 2008).

Table 3: Performance Metrics for X, Y, Z axes individually.

	X (lateral)				Y (head-to-foot)				Z (dorso-ventral)			
	AR	AS	MR	MS	AR	AS	MR	MS	AR	AS	MR	MS
Accuracy	0.92	0.91	0.90	0.93	0.91	0.90	0.90	0.93	0.92	0.93	0.92	0.95
Precision (macro)	0.92	0.91	0.90	0.91	0.92	0.90	0.90	0.90	0.93	0.93	0.92	0.95
Precision (weighted)	0.92	0.91	0.90	0.93	0.91	0.90	0.90	0.92	0.92	0.93	0.92	0.95
Recall (macro)	0.89	0.90	0.90	0.86	0.87	0.90	0.90	0.86	0.90	0.92	0.92	0.88
Recall (weighted)	0.92	0.91	0.90	0.93	0.91	0.90	0.90	0.93	0.92	0.93	0.92	0.95
f1-score (macro)	0.91	0.90	0.90	0.89	0.89	0.90	0.90	0.88	0.91	0.93	0.92	0.91
f1-score (weighted)	0.92	0.91	0.90	0.93	0.90	0.90	0.90	0.93	0.92	0.93	0.92	0.95
ROC AUC	0.89	0.90	0.90	0.86	0.87	0.90	0.90	0.86	0.89	0.92	0.92	0.88

3.2 Classification Results

Following feature elimination, an XGBoost-based multi-label/multi-class classification framework leveraging *One vs. Rest* strategy was built. To assess the model performance, accuracy, precision, recall, f1-score and ROC AUC metrics were calculated. The multi-label/multi-class classification results, corresponding ROC curves and confusion matrices for each VHD are presented in Table 2 and Fig. 4. As seen, for all four VHDs, the accuracy, weighted precision, weighted recall and weighted f1-score values were above 95%. Additionally, the average ROC AUC value for all four VHDs was calculated as 0.95 (Fig. 4). Obtaining superior performance values shows that the spectral features and the XGBoost-based multi-label/multi-class classification framework work at sufficiently high performance.

3.3 Axis Interpretation

As the last analysis, the aforementioned analysis pipeline was repeated on the X, Y and Z axes individually. Initially, there were 2499 features extracted from each of the lateral (X), head-to-foot (Y), and dorso-ventral (Z) axes. For the X axis, this number decreased to 252 following p-value analysis and to 143 after variance thresholding. Similarly for Y and Z axes, these values were 256 to 131 and 253 to 159, respectively. For each axis, a separate model was trained and tested. The multi-label/multi-class classification results are presented in Table 3. As expected, the classifier performances were lower compared to the case where features from all three axes were used, however still most of the performance values were above 90%. The best performing axis was found to be the dorso-ventral direction (Z), which has indeed been the most commonly used axis in cardiovascular health assessment (Taebi et al., 2019).

4 CONCLUSIONS

In this paper, an XGBoost-based multi-label/multi-class classification framework was proposed to distinguish between aortic stenosis (AS), aortic valve regurgitation (AR), mitral valve stenosis (MS), and mitral valve regurgitation (MR) using the tri-axial SCG signals collected from the mid-sternum. First, seismology domain knowledge was leveraged and applied to SCG signals through ObsPy toolbox for pre-processing. From pre-processed signal segments, spectrogram, wavelet, chromagram, tempogram and zero-crossing-rate features were extracted. Following p-value analysis and variance thresholding, a multi-label/multi-class classification framework based on gradient boosting trees was developed to distinguish between AS, AR, MS and MR cases.

For all four VHDs, the accuracy, weighted precision, weighted recall and weighted f1-score values were above 95%. In addition, when the SCG axes were investigated individually, it was found that the features extracted from the dorso-ventral direction (Z axis) shows superior performance compared to other two axes. Overall, the results showed that spectral analysis of SCG signals can provide valuable information regarding VHDs and potentially be used in the design of continuous monitoring systems. Future work will focus on validating these findings in larger datasets and improving the current pipelines further to achieve real-time VHD detection and assessment.

REFERENCES

Beyreuther, M., Barsch, R., Krischer, L., Megies, T., Behr, Y., and Wassermann, J. (2010). Obspy: A python toolbox for seismology. *Seismological Research Letters*, 81(3):530–533.

Bommert, A., Sun, X., Bischl, B., Rahnenführer, J., and Lang, M. (2020). Benchmark for filter methods for feature selection in high-dimensional classifica-

tion data. *Computational Statistics & Data Analysis*, 143:106839.

Chen, L. (2009). Curse of dimensionality. encyclopedia of database systems.

Dietterich, T. G. et al. (2002). Ensemble learning. *The handbook of brain theory and neural networks*, 2(1):110–125.

Giannakopoulos, T. and Pikrakis, A. (2014). *Introduction to audio analysis: a MATLAB® approach*. Academic Press.

Go, A. S., Mozaffarian, D., Roger, V. L., Benjamin, E. J., Berry, J. D., Borden, W. B., Bravata, D. M., Dai, S., Ford, E. S., Fox, C. S., et al. (2013). Heart disease and stroke statistics—2013 update: a report from the american heart association. *Circulation*, 127(1):e6–e245.

Golubnitschaja, O., Kinkorova, J., and Costigliola, V. (2014). Predictive, preventive and personalised medicine as the hardcore of 'horizon 2020': Epma position paper. *EPMA Journal*, 5(1):1–29.

Hersek, S., Pouyan, M. B., Teague, C. N., Sawka, M. N., Millard-Stafford, M. L., Kogler, G. F., Wolkoff, P., and Inan, O. T. (2017). Acoustical emission analysis by unsupervised graph mining: A novel biomarker of knee health status. *IEEE Transactions on Biomedical Engineering*, 65(6):1291–1300.

Hurnanen, T., Lehtonen, E., Tadi, M. J., Kuusela, T., Kiviniemi, T., Saraste, A., Vasankari, T., Airaksinen, J., Koivisto, T., and Pänkäälä, M. (2016). Automated detection of atrial fibrillation based on time–frequency analysis of seismocardiograms. *IEEE journal of biomedical and health informatics*, 21(5):1233–1241.

Imirzalioglu, M. and Semiz, B. (2022). Quantifying respiration effects on cardiac vibrations using teager energy operator and gradient boosted trees. In *2022 44th Annual International Conference of the IEEE Engineering in Medicine & Biology Society (EMBC)*, pages 1935–1938. IEEE.

Inan, O. T., Baran Pouyan, M., Javaid, A. Q., Dowling, S., Etemadi, M., Dorier, A., Heller, J. A., Bicen, A. O., Roy, S., De Marco, T., et al. (2018). Novel wearable seismocardiography and machine learning algorithms can assess clinical status of heart failure patients. *Circulation: Heart Failure*, 11(1):e004313.

Inan, O. T., Migeotte, P.-F., Park, K.-S., Etemadi, M., Tavakolian, K., Casanella, R., Zanetti, J., Tank, J., Funtova, I., Prisk, G. K., et al. (2014). Ballistocardiography and seismocardiography: A review of recent advances. *IEEE journal of biomedical and health informatics*, 19(4):1414–1427.

Jahromi, M. G., Parsaei, H., Zamani, A., and Dehbozorgi, M. (2017). Comparative analysis of wavelet-based feature extraction for intramuscular emg signal decomposition. *Journal of biomedical physics & engineering*, 7(4):365.

Klabunde, R. (2011). *Cardiovascular physiology concepts*. Lippincott Williams & Wilkins.

Koutroumbas, K. and Theodoridis, S. (2008). *Pattern recognition*. Academic Press.

Lay, T. and Wallace, T. C. (1995). *Modern global seismology*. Elsevier.

Levin, H. S., Runco, V., Goodwin, R. S., Ryan, J. M., et al. (1962). The effect of respiration on cardiac murmurs: An auscultatory illusion. *The American Journal of Medicine*, 33(2):236–242.

McClellan, J. H., Schafer, R. W., and Yoder, M. A. (2003). *Signal processing first*. Pearson education Upper Saddle River, NJ.

Meister, S., Deiters, W., and Becker, S. (2016). Digital health and digital biomarkers–enabling value chains on health data. *Current Directions in Biomedical Engineering*, 2(1):577–581.

Pandia, K., Inan, O. T., Kovacs, G. T., and Giovangrandi, L. (2012). Extracting respiratory information from seismocardiogram signals acquired on the chest using a miniature accelerometer. *Physiological measurement*, 33(10):1643.

Polikar, R. (1996). The wavelet tutorial second edition part i. *Fundamental Concepts & An Overview of The Wavelet Theory*.

Sedgwick, P. (2015). A comparison of parametric and non-parametric statistical tests. *BMJ*, 350.

Semiz, B., Carek, A. M., Johnson, J. C., Ahmad, S., Heller, J. A., Vicente, F. G., Caron, S., Hogue, C. W., Etemadi, M., and Inan, O. T. (2020). Non-invasive wearable patch utilizing seismocardiography for perioperative use in surgical patients. *IEEE Journal of Biomedical and Health Informatics*, 25(5):1572–1582.

Shah, A., Kattel, M., Nepal, A., and Shrestha, D. (2019). Chroma feature extraction. *Chroma Feature Extraction using Fourier Transform*.

Shandhi, M. M. H., Semiz, B., Hersek, S., Goller, N., Ayazi, F., and Inan, O. T. (2019). Performance analysis of gyroscope and accelerometer sensors for seismocardiography-based wearable pre-ejection period estimation. *IEEE journal of biomedical and health informatics*, 23(6):2365–2374.

Svensson, L. (2008). Aortic valve stenosis and regurgitation: an overview of management. *Journal of Cardiovascular Surgery*, 49(2):297.

Taebi, A., Solar, B. E., Bomar, A. J., Sandler, R. H., and Mansy, H. A. (2019). Recent advances in seismocardiography. *Vibration*, 2(1):64–86.

WHO (2020). The top 10 causes of death. *Geneva: World Health Organization*. https://www.who.int/newsroom/fact-sheets/detail/the-top-10-causes-of-death (visited: 2022-09).

Yang, C., Aranoff, N. D., Green, P., and Tavassolian, N. (2019). Classification of aortic stenosis using time–frequency features from chest cardio-mechanical signals. *IEEE Transactions on Biomedical Engineering*, 67(6):1672–1683.

Yang, C., Fan, F., Aranoff, N., Green, P., Li, Y., Liu, C., and Tavassolian, N. (2021). An open-access database for the evaluation of cardio-mechanical signals from patients with valvular heart diseases. *Frontiers in Physiology*, 12.